mater.scichina.com link.springer.com

Sci China Mater 2025, 68(10): 3657–3666
https://doi.org/10.1007/s40843-025-3504-1

Enhanced OH^- conductivity and alkaline stability of AEM by pyrene stacking backbone for water electrolysis

Cui Yang[1†], Yu Huang[2†], Wanjie Song[1], Mingyue Wu[1], Jinyu Nie[1], Yaoming Wang[1], Liang Wu[1], Xiaolin Ge[1*] and Tongwen Xu[1*]

ABSTRACT A burgeoning hydrogen technology utilizing anion exchange membranes (AEMs) has attracted increasing interest owing to its potential for cost-effective commercial values. Nonetheless, there are still challenges pertaining to conductivity and persistent stability. Herein, an innovative approach has been introduced to enhance the alkaline resistance and conductivity of AEMs via π-π interactions. The synergistic π-stacking networks in the polymer backbone induce long-range cation aggregation through directed self-assembly, generating ionic cluster microdomains. These nanoconfined environments elevate local hydroxide concentration, leading to the increased density of accessible ion hopping sites within the localized regions. Furthermore, the electron-donating effects of pyrene effectively reduce the electrostatic potential of the β-H adjacent to quaternary ammonium cations, thus increasing the energy barrier for OH^- nucleophilic attack. The obtained AEMs demonstrate exceptional performance, exhibiting both high conductivity (160 mS/cm) and excellent alkaline stability (merely 0.35% conductivity degradation after 1950 h in 2 M KOH at 80 °C). These good properties enable the membrane electrode assembly (MEA) to achieve the current density of 2.58 A/cm^2 at 1.8 V, while maintaining stable operation for over 700 h in durability testing.

Keywords: anion exchange membranes, water electrolysis, π-π stacking, high alkaline resistance, electron-donating effect

INTRODUCTION

Water electrolysis technology powered by renewable energy sources has emerged as a pivotal solution for large-scale green hydrogen production, offering a sustainable pathway for future energy systems [1]. Among various electrolysis technologies, anion exchange membrane water electrolyzers (AEMWEs) exhibit distinct advantages, including the utilization of non-precious metal catalysts and rapid start-stop capabilities, making them extremely suitable for integration with intermittent renewable energy systems. These advantages make AEMWEs a promising alternative to both alkaline water electrolyzers (AWEs) and proton exchange membrane water electrolyzers (PEMWEs) [2]. As a core component of AEMWEs, AEMs critically influence device performance [3], impelling extensive research into developing membranes with high ionic conductivity and excellent chemical stability [4–10].

After decades of research, a consensus has emerged that chemically integrating heteroatom-free linkage backbones with stable cationic groups represents a reliable approach for developing stable AEMs [11–15]. A prominent case is the poly(aryl piperidine) (PAP) AEMs, synthesized through Friedel–Crafts polycondensations of *N*,*N*-dimethyl piperidiniums (DMPs) with aromatic monomers [16]. The enhanced alkaline stability of piperidinium cation is widely attributed to their reduced ring strain and effective steric hindrance inhibition [17,18]. Although various aromatic monomers have been employed to enhance the conductivity of PAP membranes, investigations into corresponding AEMs with different aromatic units have revealed inconsistent stability trends [7,19–21]. Moreover, the correlation between aromatic monomer structures and membrane stability remains insufficiently explored. Hence, systematic investigation into the influence of monomer units on ring stability is both necessary and scientifically significant. Previous studies have confirmed that modulating the electronic effect of monomers surrounding functional groups can effectively enhance their chemical stability [22–24]. For instance, He's group [25] demonstrated that reducing the electrostatic potential (ESP) of β-H through electron-donating effect can effectively improve the alkaline-resistant stability of AEMs. This finding suggests that incorporating electron-donating aromatic units into PAPs could further optimize the alkaline stability of AEMs.

Moreover, high ion conductivity serves as a foundation prerequisite for AEMWEs to achieve high current density operation [26,27]. However, the inherent lack of self-assembly driving forces in macromolecules typically results in substantial channel curvatures and elevated ion conduction energy barriers. Abundant studies have consistently shown that facilitating cation aggregation through enhancing side chain mobility can effectively address these limitations. Zhang *et al.* [28] successfully engineered ordered ion channels in anion exchange membranes via cation-dipole interaction, demonstrating significantly accelerated OH^- conduction. Nevertheless, the inherent randomness of polymer backbones typically leads to excessive zigzag configurations, which significantly impede efficient ion transport. A breakthrough by Winey's group [29] demonstrated that precisely

[1] Key Laboratory of Precision and Intelligent Chemistry, Department of Applied Chemistry, School of Chemistry and Materials Science, University of Science and Technology of China, Hefei 230026, China
[2] Department of Polymer Science and Engineering, University of Science and Technology of China, Hefei 230026, China
[†] Equally contributed to this work.
[*] Corresponding author (email: gexl@ustc.edu.cn; twxu@ustc.edu.cn)

controlled chain folding can dramatically enhance proton conductivity. These findings establish polymer backbone topology manipulation as a highly effective strategy for constructing highway ion transport channels. Furthermore, inducing backbone self-assembly via non-covalent interactions presents a promising approach to mitigate excessive chain disordered entanglement.

Pyrene, renowned for its electron-rich properties and extensive π-conjugated aromatic structure, has been widely employed in optical applications [30–32]. In this work, we strategically incorporated pyrene into AEMs to implement dual functional strategies: (1) the integration of electron-donating units adjacent to DMP groups serves to reduce the electrostatic potential of β-H, thereby enhancing degradation resistance through elevated energy barriers against OH^- attack; (2) the strong π-π interactions between the extended π-conjugated aromatic systems facilitate polymer backbone self-assembly, enabling the formation of well-ordered ion channels. These features establish pyrene units as highly effective building blocks for advanced AEMs fabrication. Through comprehensive structural characterization and systematic performance evaluation, the QPBF-*x* membranes have demonstrated good properties, highlighting their significant potential for AEMWE applications.

EXPERIMENTAL SECTION

Materials

Pyrene, biphenyl, 2,2,2-trifluoroacetophenone, *N*-methyl-4-piperidone, trifluoroacetic acid (TFA), trifluoromethanesulfonic acid (TFSA) and methyl iodide (CH_3I) were purchased from Energy Chemical Co., Ltd. (Shanghai, China). Dichloromethane (DCM), dimethyl-sulfoxide (DMSO) and potassium hydroxide (KOH) were purchased from Sinopharm Chemical Reagent Co., Ltd. (Shanghai, China). All the reagents were used as received without further purification.

Synthesis of poly(pyrene-*co*-biphenyl-trifluoroacetophenone-*co*-(*N*-methyl-4-piperidone)) (PBF-*x*) copolymer

The polymer backbone of QPBF-*x* was synthesized through superacid catalyzed polymerization, where *x* meant the mole ratio of pyrene units. In order to ensure the mechanical properties and dimensional stability of the membranes, appropriate ion exchange capacity (IEC) was regulated by the ratio of the 2,2,2-trifluoroacetophenone to *N*-methyl-4-piperidone. Take the synthesis routine of QPBF-20 AEM as an example. Pyrene (0.41 g, 2 mmol), biphenyl (1.23 g, 8 mmol), 2,2,2-trifluoroacetophenone (0.73 g, 4.2 mmol) and *N*-methyl-4-piperidone (0.88 g, 7.8 mmol) were dissolved in DCM (4 mL) in ice bath. Then 1.2 mL TFA and 9 mL TFSA were added slowly to the mixed solution. When the reaction reached the highest viscosity of the solution (about 5 h) in the ice bath, the mixture was poured into water and sunk to stop the reaction. The sunk polymer was washed to a neutral state and dried overnight under 60 °C. The neutral polymer was deprotonated with 2 M KOH aqueous solution for 48 h, then washed to neutral state, dried overnight and collected. The ^{1}H nuclear magnetic resonance (NMR) spectra of PBF-*x* were shown in Figs S2–S4.

Synthesis of quaternized poly(pyrene-*co*-biphenyl-trifluoroactophenone-*co*-(*N*-methyl-4-piperidone)) (QPBF-*x*) copolymer

Neutral polymer backbone (0.5 g), CH_3I (0.5 mL) and DMSO (6 mL) were mixed and stirred without light under 30 °C for 24 h. And a dark brown clarified solution was obtained. The clear solution was poured into acetone to sink out the polymer and the quaternized polymer was washed until the filtrate was colorless. Then it was washed in deionized water and dried overnight. The ^{1}H NMR spectra of QPBF-*x* were shown in Fig. 1b.

Casting of QPBF-*x* membranes

Firstly, the QPBF-*x* copolymer (0.2 g) was dissolved in 7 mL DMSO and the solution was filtered with a filter (0.45 μm). The obtained yellow clarified solution was cast on a 7 cm×7 cm cast film plate, and then evaporated slowly at 70 °C over one day. The QPBF-*x* membranes were peeled carefully after being immersed in deionized water. The obtained membrane was immersed in 1 M KOH for 24 h to change ion form from I^- to OH^-.

Computation details

The Gaussian 16 program was used to perform the density functional theory (DFT) calculations. The hybrid exchange-correlation functional B3LYP with D3 empirical dispersion corrections with Becke-Johnson damping and 6-311G(d) basis set was employed in all calculations. The ESP analysis was carried out by Multiwfn dev3.8 software [33] based on the optimized structure, and the visualization of ESP was done through VMD software. The independent gradient model based on Hirshfeld partition (IGMH) introduced by Lu and Chen [34] was used to visualize the interaction between molecules.

Characterization

IEC. The IEC practical values of the QPBF-*x* AEMs were measured by mole titration. AEMs were set in 1 M KCl aqueous solution for 24 h in 60 °C to ensure complete ion exchange. Then, AEMs were washed several times and immersed in deionized water for 24 h to remove the redundant Cl^- on surface. It was dried for 24 h to remove the redundant water, weighed and recorded as *W*, and immersed in 1 M KNO_3 aqueous solution for 24 h under 60 °C to replace Cl^-. This solution was titrated with 0.01 M $AgNO_3$ solution, and the volume of $AgNO_3$ is recorded as *V*. The calculation Equations of IEC were

$$\mathrm{IEC}_{Cl^-} = \frac{0.01V}{W}, \tag{1}$$

$$\mathrm{IEC}_{OH^-} = \frac{0.01V}{W-0.185V}. \tag{2}$$

Water uptake (WU) and swelling ratio (SR). The QPBF-*x* AEMs were immersed in 1 M KOH for 24 h to exchange the accompanying ions to OH^-. Then AEMs were washed with deionized water, immersed in deionized water and kept at different temperatures for 12 h. The weight (W_x), length (L_x) and temperature (T_0) were quickly recorded when drying the moisture on the surface of the film. Finally, the AEMs were dried 48 h under 60 °C. The weight (W_0) and length (L_0) of the dry film were measured. And the WU (Equation (3)) and SR (Equation (4)) were calculated by

$$\mathrm{WU} = \frac{W_x - W_0}{W_0}, \tag{3}$$

$$\mathrm{SR} = \frac{L_x - L_0}{L_0}. \tag{4}$$

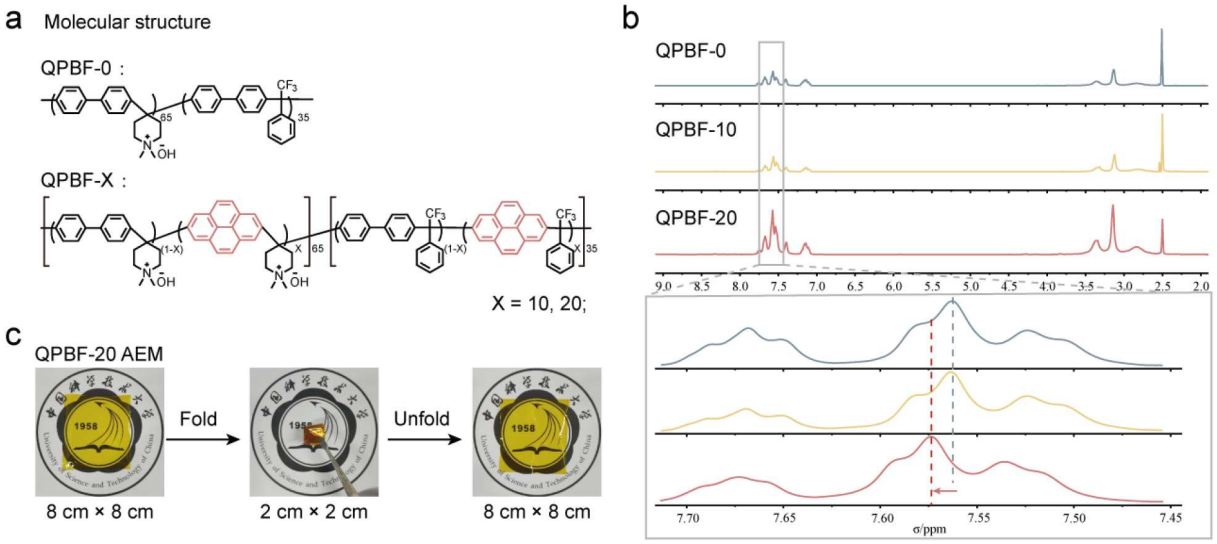

Figure 1 (a) Molecular structure of QPBF-*x* polymers; (b) ^{1}H NMR of QPBF-*x* polymers; (c) folded-unfold pictures of QPBF-20 membrane.

Ionic conductivity. The in-plane OH^- ion conductivity of QPBF-*x* AEMs was measured on AC impedance analyzer (Zahner Zennium E) via a four-electrode method on a platinum electrode. The distance between the two potential sensing electrolytes (L), width (w) and thickness (d) of the AEMs were quickly recorded. The resistance (R) was collected over the frequency range from 1 MHz to 100 Hz at a set temperature. The conductivity (σ) was calculated by

$$\sigma = \frac{L}{w \times d \times R}. \quad (5)$$

Activation energy (E_a) of OH^- was calculated by the Arrhenius equation:

$$\ln\sigma = \ln\sigma_0 - \frac{E_a}{k}\frac{1}{T}, \quad (6)$$

where σ is the OH^- conductivity of AEMs, σ_0 is pre-exponential factors, k is Boltzmann constant, and T is the absolute temperature (K).

Ex-situ durability. The QPBF-0 and QPBF-20 AEMs were immersed in 2 M KOH aqueous solution at 80 °C and changes in conductivity were monitored.

^{1}H NMR spectrum. The spectra were recorded on a Bruker 510 instrument (400 MHz). $CDCl_3$-*d* and DMSO-d_6 were used as the solvents with TMS as the internal standard.

RESULTS AND DISCUSSION

Synthesis and characterization

The polymer structure and synthesis route of QPBF-*x* membranes are schematically illustrated in Fig. 1a and Fig. S1. The synthesis of QPBF-*x* AEMs was accomplished via a two-step procedure. Initially, the polymer backbone was synthesized via Friedel-Crafts alkylation using pyrene, biphenyl and *N*-methyl-4-piperidone as monomers. The successful incorporation of pyrene units was confirmed by ^{1}H NMR spectra (Figs S2–S4), where characteristic aromatic proton signals emerged in the chemical shift range of 7.75–8.50 ppm. Subsequently, QPBF-*x* was obtained through quaternization with methyl iodide via the Menshutkin reaction, where *x* denotes the average molar fraction of pyrene units in the copolymer. The chemical structure of the synthesized QPBF-*x* was confirmed by ^{1}H NMR spectra, as shown in Fig. 1b. The resulting anion exchange membranes, exhibiting a distinct yellow coloration (Fig. 1c), demonstrated remarkable flexibility, as evidenced by their ability to undergo complete folding and restoration in the dry state.

Construction of well-defined ion channels deriving from π-π stacking

Generally, the phase separation between hydrophilic and hydrophobic domains driven by the differences in hydrophilicity and hydrophobicity of polymer backbone and cation groups facilitates the formation of ion channels through cation aggregation. However, the driving force behind cation aggregation is governed by thermodynamics, which is inherently weak and uncontrollable. Commonly, large π-conjugated molecules tend to orderly stacking due to the presence of π-π interactions. Therefore, the introduction of pyrene into the polymer offers the potential to drive the backbones to stack to form ordered channels.

The π-π stacking interactions among pyrene units in QPBF-*x* polymer were systematically characterized using X-ray diffraction (XRD). In addition, as shown in Fig. 2a, a distinct peak at 2θ = 28° is evident in the XRD pattern of the QPBF-20 membranes. This peak indicates that the pyrene units within the AEM have established an effective π-π stacking structure, driven by the robust π-π stacking interactions of the pyrene rings. The resulting backbones packing enhanced the formation of well-defined ion channels. However, random copolymers inherently lack long-range ordered stacking architectures compared to small-molecule crystals or semi-crystalline polymers (e.g., polyethylene). Their disordered chain arrangements typically lead to broadened XRD peaks due to limited coherent scattering domains and reduced diffraction intensity from weakened periodicity. This intrinsic structural characteristic is consistent with the observed XRD pattern in our study. The calculated π-π stacking distance, derived from the Bragg equation ($2d\sin\theta = n\lambda$) is 3.2 Å. In contrast, the XRD pattern of the QPBF-0 membranes exhibits only a faint protrusion at 2θ = 28° (Fig. 2d), suggesting that biphenyls have insufficient driving force to induce the formation of a well-defined stacking structure within the back-

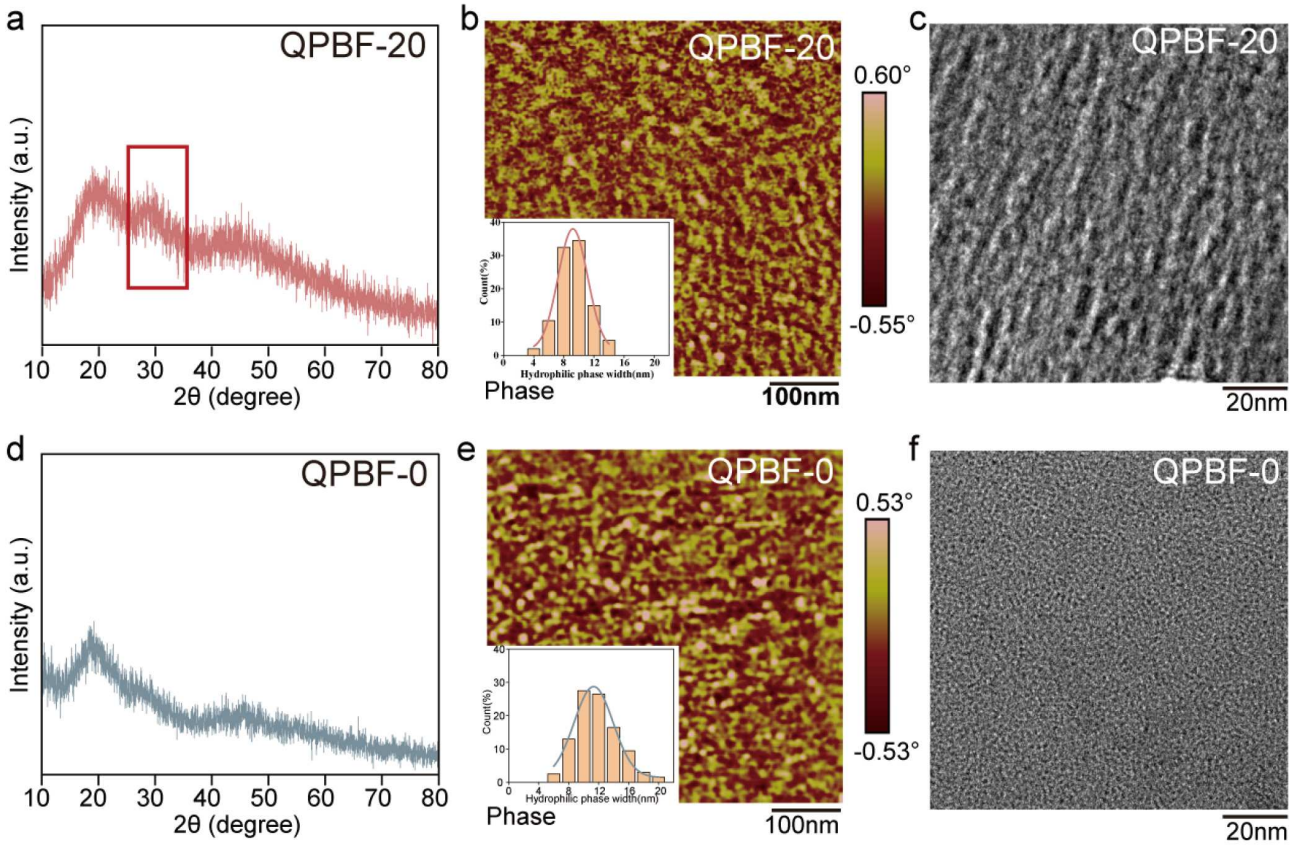

Figure 2 (a, d) XRD patterns, (b, e) AFM images in tapping mode (the insets in the lower left corner were the size distribution statistics of the hydrophilic areas) and (c, f) TEM images of QPBF-20 and QPBF-0 AEM.

bone.

We investigated the morphology control effect of the structural features of QPBF-*x* via nanoscale microscopy analysis using transmission electron microscopy (TEM) and atomic force microscopy (AFM). As displayed in Fig. 2b, distinct microphase-separation morphologies are evident in the AFM images, where the dark regions represent the aggregated quaternary amine groups. By analyzing 200 random points, the size distributions of the hydrophilic areas were calculated, as shown in the lower left corner of Fig. 2b, e. The size distribution of both the hydrophobic phase (light areas) and hydrophilic phase (dark areas) in the QPBF-20 membrane (Fig. 2b) falls within a narrow range from 8 to 12 nm, with the average size of the hydrophilic phase being approximately 10 nm. This narrow distribution suggests the presence of periodically arranged cation clusters, highlighting the well-defined microphase separation in the membrane. More notably, TEM analysis reveals the presence of periodically distributed cation clusters, highlighting a unique cation aggregation behavior. This contrasts with most reported methods, which typically rely on modulating side chain flexibility to control cation aggregation. Our findings demonstrate that the intermolecular π-π interactions within the main chain serve as a more robust driving force, promoting orderly cation aggregation and enabling the construction of well-defined ion transport channels. In contrast, the QPBF-0 membrane, as a control sample, exhibits poor self-assembly ability, characterized by a broader and more dispersed size distribution range from 8 to 14 nm (Fig. 2e). This phenomenon arises due to the insufficient driving force for the aggregation of isolated quaternary amine groups. Both the AFM and TEM images align well with the XRD patterns. The observed striation morphologies represent the formation of well-ordered ion channels, driven by strong π-π stacking interactions. These ordered channels reduce the tortuosity of ion transport pathways, thereby facilitating rapid ion conduction. In contrast, the QPBF-0 membranes exhibit more disordered ion channels, which impede ion transmission efficiency, as shown in Fig. 2f. These observations provide compelling visual evidence of the strong π-π stacking interactions between pyrene units, confirming the successful construction of regular ion channels.

Evaluation of properties on QPBF-*x* AEMs

To investigate the role of π-π stacking in improving the performance of AEMs, the fundamental properties of QPBF-*x* AEMs were systematically evaluated. The IEC values of the QPBF-*x* AEMs were titrated repeatedly via Mohr titration. As summarized in Table S1, the IEC values for the three AEMs are 2.11, 2.10 and 2.09 mmol/g, respectively. These nearly identical IEC values eliminate the influence of IEC variations on membrane performance. Hydroxide conductivity measurements were conducted in deionized water, revealing that the conductivity of the QPBF-*x* membranes consistently increased with temperature (Fig. 3a and Table S2). This trend can be attributed to the accelerated migration rate of the hydroxide ion at elevated

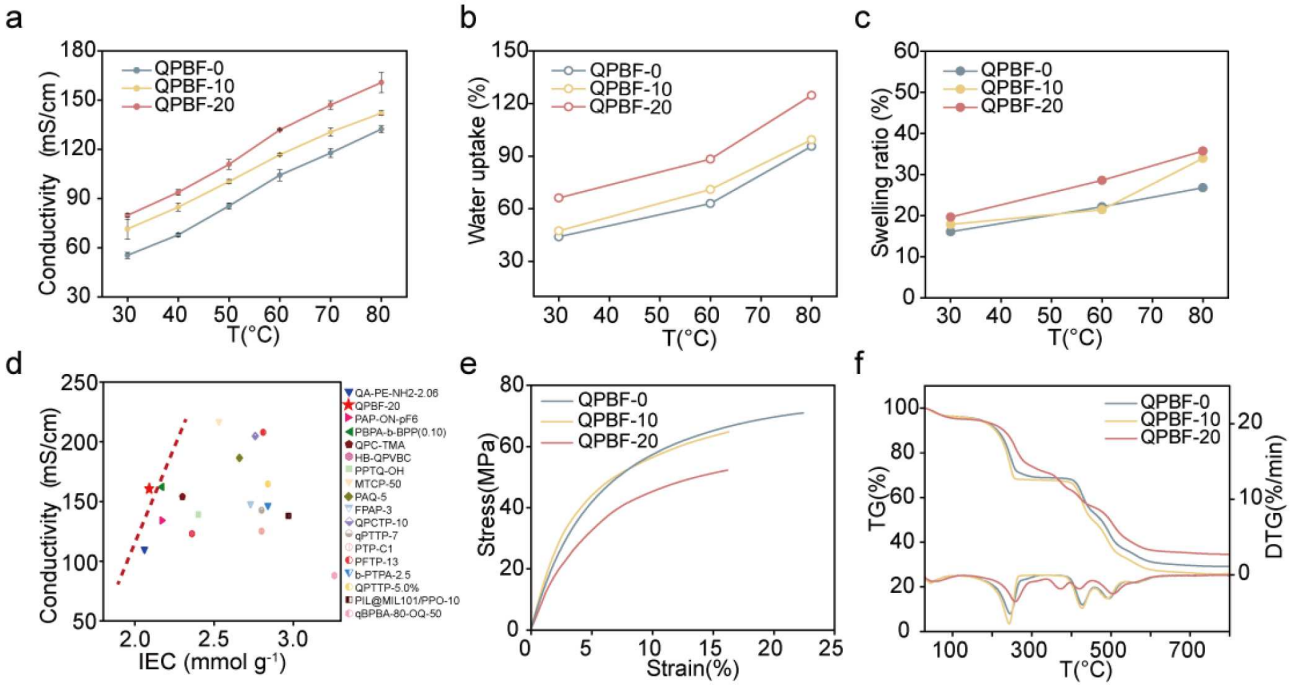

Figure 3 (a) OH^- ion conductivity of QPBF-*x* AEMs at different temperatures; (b) water uptakes and (c) swelling ratio of QPBF-*x* AEMs in OH^- form at different temperatures; (d) OH^- conductivity (80 °C) versus IEC of the QPBF-20 AEM and recently reported poly(aryl piperidinium)-based AEMs; (e) mechanical properties of QPBF-*x* in the dry state; (f) TG & DTG curves of QPBF-*x* AEMs.

temperature. In addition, across the whole temperature range (30–80 °C), the QPBF-20 AEMs exhibit the highest OH^- ion conductivity, reaching 79.7 mS/cm at 30 °C and 160.7 mS/cm at 80 °C, outperforming the other two AEMs. In comparison, the conductivity of QPBF-0 AEMs exhibited 55.3 mS/cm at 30 °C and 132.3 mS/cm at 80 °C, while the QPBF-10 AEMs showed intermediate conductivity of 71.4 mS/cm at 30 °C and 142 mS/cm at 80 °C. The E_a of ion transport of QPBF-*x* AEM is calculated by the Arrhenius equation. And the E_a of QPBF-*x* AEMs were 15.195 (QPBF-0), 13.282 (QPBF-10) and 12.647 (QPBF-20) kJ/mol. With the increase of pyrene content, the π-stacking in AEMs induced cation aggregation to promote the formation of microphase separation morphology, which enhanced local ion concentration to strengthen ion surface-hopping sites. It built effective hydrophilic ion transport channels, which can decrease the tortuosity of ion transport pathways to reduce ion transport energy barrier and improve conductivity. Therefore, the OH^- conductivity consistently increases with higher pyrene content, attributed to the more ordered ion channels in QPBF-20 and QPBF-10 AEMs.

In addition to ion channels, water, as a crucial medium for ion transport, also plays a significant role in influencing ion conduction. We further investigated the water absorption behavior of the QPBF-*x* AEMs. As shown in Fig. 3b, the water uptake follows the order of QPBF-0 (44.0%, 95.6%) < QPBF-10 (47.4%, 99.4%) < QPBF-20 (66.2%, 124.7%) at both 30 and 80 °C. This trend indicates that the stronger self-assembly driving force facilitates the interconnection of isolated hydrophilic clusters, forming continuous ion channels and increasing the absorption and uniform distribution of water. The swelling test results reveal that the swelling ratios all fall within an acceptable range, as shown in Fig. 3c. Given the operation demands of AEMs, their mechanical strength, thermostability and dimension stability are also critical. As shown in Fig. 3e, the QPBF-*x* AEMs exhibit tensile strengths exceeding 50 MPa and elongations at break exceeding 15%, demonstrating their sufficient mechanical strength and flexibility to meet the requirements for device assembly. Regarding thermostability, the thermogravimetry (TG) and differential thermogravimetry (DTG) data in Fig. 3f indicate that the QPBF-*x* AEMs all possess decomposition temperatures above 200 °C, satisfying the operational temperature range of 60–90 °C. In addition, the QPBF-20 AEMs achieve higher conductivity than many existing AEMs at a lower IEC, enabling them to attain superior conductivity with minimal swelling, as shown in Fig. 3d [21,25,35–49]. These fundamental properties collectively establish a robust foundation for the efficient performance of QPBF-20 AEMs in AEMWEs.

Enhancing alkaline stability via the electron-donating effect

To ensure efficient and stable operation of AEMWEs under high-temperature and harsh alkaline conditions, AEMs must possess not only high OH^- ion conductivity but also sufficient alkali resistance. In this study, the incorporation of pyrene units significantly enhanced the conductivity of QPBF-20 AEMs. To assess the alkaline stability of the QPBF-*x* AEMs under operation conditions, accelerated alkaline stability tests were conducted by immersing QPBF-0 and QPBF-20 AEMs in 2 M KOH at 80 °C. As shown in Fig. 4a, QPBF-20 AEMs demonstrated exceptional stability, remaining 99.65% of their initial conductivity after 1950 h of alkaline exposure, with negligible degradation. In contrast, QPBF-0 AEM exhibited a substantial conductivity loss, retaining only 77.26% of their initial conductivity after 1600 h. ^{1}H NMR spectrum was employed to investigate the degradation mechanism. As shown in Fig. 4b and Fig. S13, the appearance of minor signals at 6.91, 5.29 and 4.93 ppm, corresponding to the β-H of piperidinium, indicates

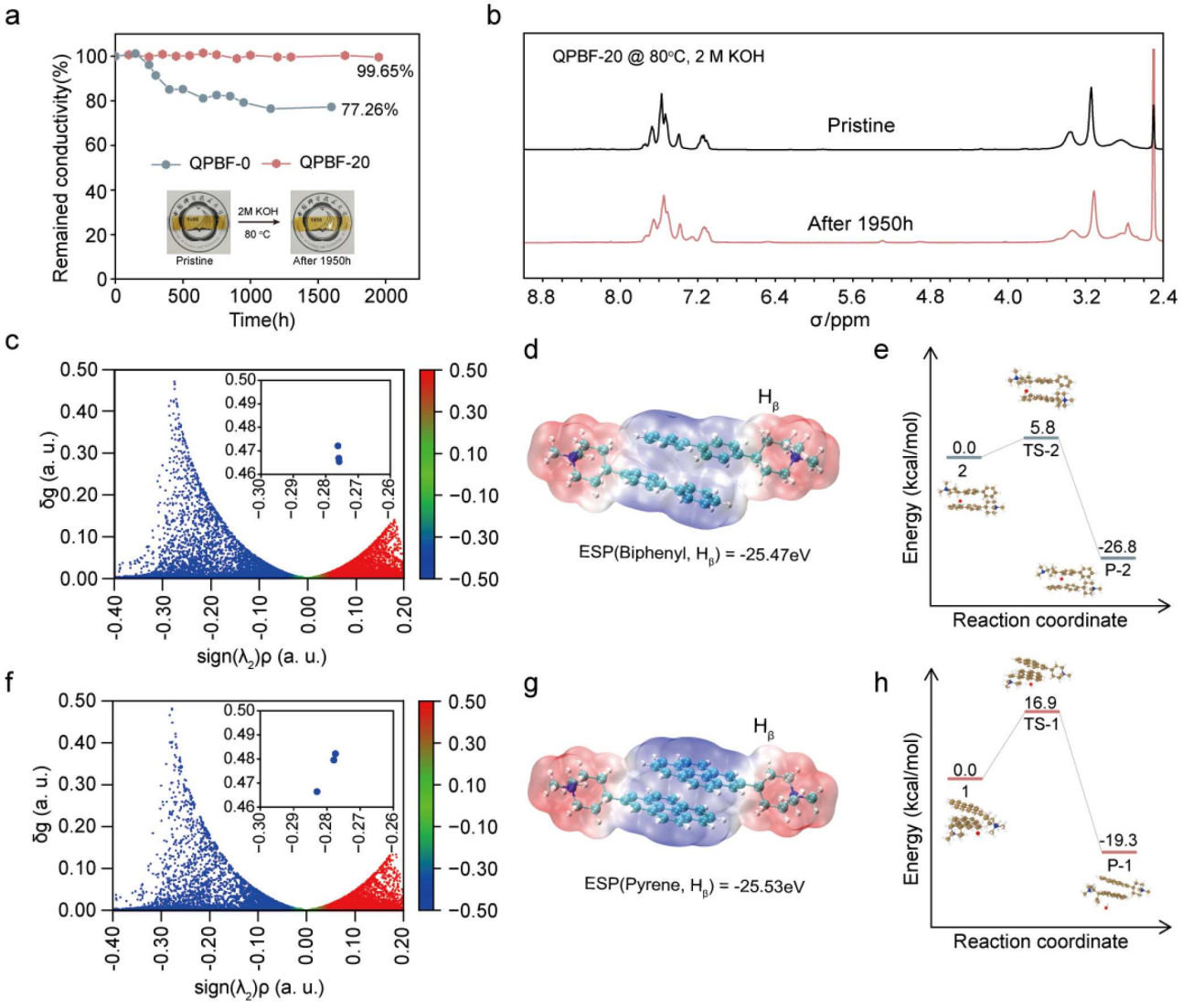

Figure 4 (a) OH^- conductivity remaining of the QPBF-0 and QPBF-20 AEMs in 2 M KOH at 80 °C; (b) ^1H NMR of the QPBF-20 AEM before and after 1950 h of alkaline stability testing; (c, f) non-covalent force between the stacked aromatic units and β-H; (d, g) electrostatic potential of β-H; (e, h) energy barriers of OH^- ions attacking the β-H of QPBF-0 and QPBF-20 AEM.

that only 0.77% Hofmann degradation occurred in the QPBF-20 AEM (Fig. S13). It is consistent with the conductivity decay rate (0.35%). This observation demonstrates the exceptional long-term alkaline stability of QPBF-20 AEM under severe operating, including high-concentration KOH solution and elevated temperature, outperforming both QPBF-0 and the majority of previously reported AEMs.

The remarkable enhancement in membrane stability induced by pyrene units motivated us to explore the underlying mechanism responsible for the significant differences in degradation behavior. Through theoretical analysis of the polymeric structure, we systematically compared pyrene-piperidinium units with biphenyl-piperidinium units as representative model systems. DFT calculations revealed stronger electrostatic interactions between pyrene and β-H, as shown in Fig. 4c. This phenomenon can be attributed to the electron-donating capability of aromatic units, which facilitates a more balanced electron distribution when conjugated with cationic groups. The extended planar π-conjugated electron cloud of pyrene endows it with superior electron-donating capability compared to biphenyl (as shown in Fig. 4f). As evidenced by the ^1H NMR spectra in Fig. 1b, the aromatic proton signals progressively move to the lower field with increasing pyrene content. This characteristic shift suggests that the combined effects of pyrene units stacking and the electron donor-acceptor interactions between pyrene units and DMP groups effectively reduce the electron density surrounding the aromatic rings. This electronic structure difference is quantitatively reflected in the DFT calculations, which show that the β-H of piperidinium adjacent to pyrene exhibits a lower electrostatic potential (−25.53 eV) than its biphenyl counterpart (−25.47 eV), as shown in Fig. 4d, g. This reduced electrostatic potential consequently decreases the reactivity of β-H in Hofmann elimination reactions. To further quantify the inhibition effect of aromatic units on Hofmann degradation, we systematically calculated the reaction energy barriers associated with OH^- ion attack on β-H. As shown in Fig. 4e, the energy barrier for OH^- attack in Hofmann elimination is significantly higher for the pyrene-adjacent structure

(16.9 kcal/mol) compared to the biphenyl-adjacent configuration (5.8 kcal/mol, Fig. 4h), representing 2.91 times increase. This substantial difference in activation energy indicates that the nucleophilic attack on β-H adjacent to pyrene is considerably more energetically demanding. These computational findings provide a fundamental explanation for the exceptional alkaline stability observed in the QPBF-20 AEM. Both experimental alkaline stability tests and theoretical calculations consistently demonstrate that the pronounced electron-donating effects of pyrene substantially enhance the alkaline resistance of AEMs.

Evaluation of performance and durability in the AEMWE system

Excellent ionic conductivity and robust alkaline stability are essential prerequisites for the long-term stable operation of AEMs in AEMWEs under harsh conditions of high temperature and alkaline environments. Recognizing the inherent differences between conventional alkaline resistance testing and actual operating conditions, it is crucial to evaluate whether QPBF-*x* AEMs can meet practical operational requirements. Therefore, we systematically assessed the water electrolysis performance of QPBF-*x* AEMs at 80 °C, maintaining consistent experimental parameters including (1) ionomeric binders (TP for anode and BP for cathode, synthesized according to a previous paper [37]), (2) catalyst loading (3 mg/cm^2 NiFe on nickel foam for anode and 1 mg/cm^2 Pt/C on carbon paper for cathode), and (3) membrane electrode assembly (MEA) preparation methods. During measurements, 1 M KOH aqueous solution was continuously circulated as the alkaline electrolyte, as shown in Fig. 5a. The resulting polarization curves, presented in Fig. 5b, demonstrate a strong correlation with the OH^- ion conductivity trends.

The current density of QPBF-*x* demonstrates a consistent

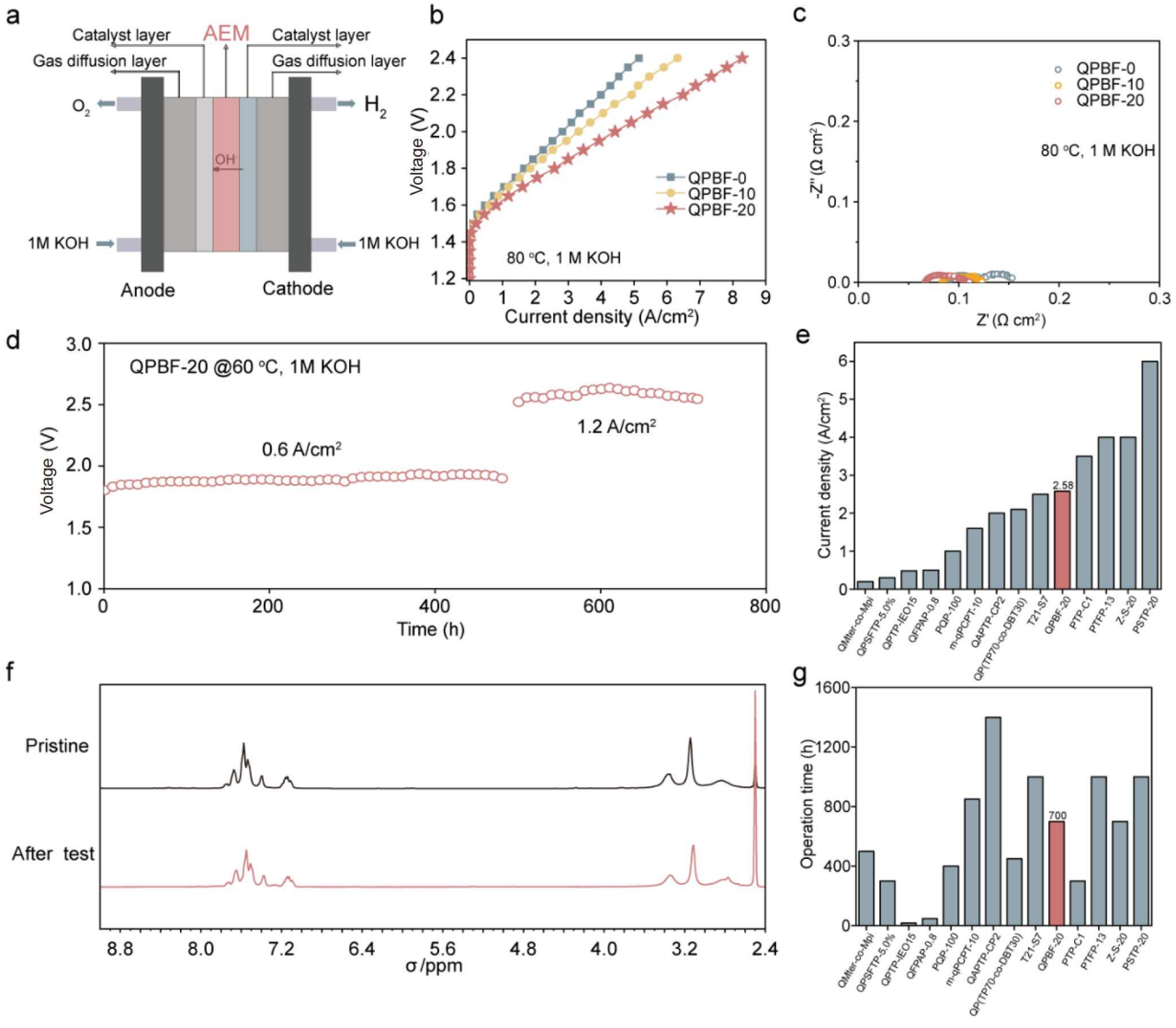

Figure 5 (a) Schematic diagram of the alkaline anion exchange membrane water electrolysis testing device; (b) current densities of QPBF-*x* AEMs in 1 M KOH at 80 °C versus the other AEMs tested in second-generation AEMWE platform; (c) EIS impedance spectra of QPBF-*x* in KOH at 80 °C with 2 A/cm^2 operation current tested in the second-generation AEMWE platform; (d) durability operation of the QPBF-20 AEM at 1 M KOH at 60 °C under a constant current state tested in the first-generation AEMWE platform; (e) current density in 1.8 V of the QPBF-20 AEM and recently reported poly(aryl piperidinium)-based AEMs in 1 M NaOH/KOH at 80 °C; (f) ^{1}H NMR of the QPBF-20 AEM before and after durability testing; (g) Durability operation time of the QPBF-20 AEM and recently reported poly(aryl piperidinium)-based AEMs.

increase with rising temperature, as evidenced by the data presented in Figs S6–S8 and Fig. S14. Remarkably, the QPBF-20 AEM achieved superior water electrolytic performance, reaching a current density of 2.58 A/cm^2 at 1.8 V in the second-generation AEMWE platform. This represents a significant enhancement, being 1.43 and 1.56 times higher than that of the QPBF-10 AEM (1.80 A/cm^2 at 1.8 V) and QPBF-0 AEM (1.65 A/cm^2 at 1.8 V), respectively. This exceptional performance can be attributed to the optimized OH^- conductivity derived from well-ordered ion channels, which promotes the rapid passage of OH^- ions by minimizing pathway tortuosity. Electrochemical impedance spectroscopy (EIS) measurements further support these findings, revealing that QPBF-20 AEM exhibits the lowest ohmic resistance of 0.067 Ω cm^2, compared to 0.084 Ω cm^2 for QPBF-10 and 0.09 Ω cm^2 for QPBF-0, as shown in Fig. 5c. The temperature-dependent EIS measurements (Figs S9–S11) confirm that this resistance trend remains consistent across various operating temperatures. These results provide compelling evidence for the effectiveness of π-π stacking in facilitating the formation of well-ordered ion channels. The long-term operational stability of AEMWEs was further evaluated through *in-situ* durability testing at 60 °C, 1 M KOH aqueous solution in the first-generation AEMWE platform, as shown in Fig. 5d. The membranes were subjected to operation at current densities of 0.6 and 1.2 A/cm^2. During the initial 500 h stability test at 0.6 A/cm^2, the system maintained good performance with small voltage fluctuations, demonstrating a low degradation rate of 0.2 mV/h. To assess the compatibility of QPBF-20 AEM with intermittent renewable resources, the current density was subsequently increased to 1.2 A/cm^2 for extended performance evaluation. Following 200 h of continuous operation at the elevated current density, the system exhibited a marginal voltage increase with a degradation rate of 0.9 mV/h, maintaining good operational stability throughout the testing period. After the durability assessment, the QPBF-20 AEM was carefully disassembled from the MEA and subjected to comprehensive structure characterization through ^{1}H NMR, as shown in Fig. 5f. The spectral analysis revealed negligible chemical degradation, confirming the exceptional alkaline stability imparted by the electron-donating characteristics of the pyrene units. This extended durability assessment underscores the practical potential of QBFF-20 AEMs in AEMWE. Comparative performance evaluation demonstrates that both electrolytic efficiency (Fig. 5e) and operation durability (Fig. 5g) of QPBF-20 AEMs are at a medium to upper level among reported PAP membranes [10,41,50–60].

CONCLUSIONS

In summary, we have developed an effective strategy for enhancing AEM performance through the incorporation of extended π-conjugated aromatic structures with pronounced electron-donating capabilities. The QPBF-20 AEM, incorporating pyrene moieties, facilitates the formation of π-π stacking via optimized electrostatic interaction, thereby promoting the self-assembly of quaternary ammonium cations into well-ordered ion channels that significantly enhance ion transport efficiency. Furthermore, the strong electron-donating characteristics of the densely packed pyrene units effectively reduce the electrostatic potential surrounding the quaternary ammonium cations, consequently increasing the activation energy barriers for E2 elimination reactions and effectively suppressing Hoffmann degradation via hydroxide ions attack. The innovative design resulted in exceptional stability, with the membrane retaining approximately 99.65% of its initial conductivity following an extensive 1950 h alkaline resistance test in 2 M KOH aqueous solution at 80 °C. The developed AEM exhibits an exceptional OH^- conductivity, remarkable stability and superior mechanical robustness. These properties collectively contributed to better AEMWE performance, achieving a current density of 2.58 A/cm^2 and demonstrating good durability over 700 h. This investigation highlights the critical role of monomer characteristics in improving membrane performance. The innovative dual-concepts approach, incorporating electron-donating interactions and π-π interactions, establishes a novel pathway for the development of high-performance AEMs.

Received 8 March 2025; accepted 20 June 2025; published online 8 September 2025

1 Terlouw T, Bauer C, McKenna R, *et al.* Large-scale hydrogen production via water electrolysis: a techno-economic and environmental assessment. Energy Environ Sci, 2022, 15: 3583–3602
2 Ham K, Bae S, Lee J. Classification and technical target of water electrolysis for hydrogen production. J Energy Chem, 2024, 95: 554–576
3 Wen J, He X, Zhang G, *et al.* Poly(aryl *N*-methyl quinuclidinium) anion exchange membrane with both ultra-high alkaline stability and dimensional stability. Sci China Mater, 2024, 67: 965–973
4 Hou J, Wang X, Liu Y, *et al.* Wittig reaction constructed an alkaline stable anion exchange membrane. J Membrane Sci, 2016, 518: 282–288
5 Li Z, Guo J, Zheng J, *et al.* A microporous polymer with suspended cations for anion exchange membrane fuel cells. Macromolecules, 2020, 53: 10998–11008
6 Liu YJ, Gao WT, Zhu AM, *et al.* High-performance di-piperidinium-crosslinked poly(*p*-terphenyl piperidinium) anion exchange membranes. J Membrane Sci, 2023, 687: 122045
7 Olsson JS, Pham TH, Jannasch P. Poly(arylene piperidinium) hydroxide ion exchange membranes: synthesis, alkaline stability, and conductivity. Adv Funct Mater, 2018, 28: 1702758
8 Song W, Liang X, Zhang H, *et al.* Ultrathin anion exchange membranes with an improved OH^- transfer rate for high-performance AEMFCs. J Mater Chem A, 2022, 10: 21503–21511
9 Xu F, Chen Y, Cao X, *et al.* Comb-shaped polyfluorene with variable alkyl chain length for application as anion exchange membranes. J Power Sources, 2022, 545: 231880
10 Zheng W, He L, Tang T, *et al.* Poly(dibenzothiophene-terphenyl piperidinium) for high-performance anion exchange membrane water electrolysis. Angew Chem Int Ed, 2024, 63: e202405738
11 Hu X, Huang Y, Liu L, *et al.* Piperidinium functionalized aryl ether-free polyaromatics as anion exchange membrane for water electrolysers: performance and durability. J Membrane Sci, 2021, 621: 118964
12 Ren R, Zhang S, Miller HA, *et al.* Facile preparation of an ether-free anion exchange membrane with pendant cyclic quaternary ammonium groups. ACS Appl Energy Mater, 2019, 2: 4576–4581
13 Wu Y, Song J, Zhao T, *et al.* Polycarbazole-based anion exchange membranes containing flexible side-chain linked piperidine pendants for alkaline fuel cells. J Membrane Sci, 2024, 707: 123031
14 Xu F, Chen Y, Lin B, *et al.* Highly durable ether-free polyfluorene-based anion exchange membranes for fuel cell applications. ACS Macro Lett, 2021, 10: 1180–1185
15 Zhang H, Wang X, Wang Y, *et al.* Alkaline-stable anion-exchange membranes with barium [2.2.2]cryptate cations: the importance of high binding constants. Angew Chem Int Ed, 2023, 62: e202217742
16 Wang J, Zhao Y, Setzler BP, *et al.* Poly(aryl piperidinium) membranes and ionomers for hydroxide exchange membrane fuel cells. Nat Energy, 2019, 4: 392–398
17 Chen N, Jin Y, Liu H, *et al.* Insight into the alkaline stability of N-heterocyclic ammonium groups for anion-exchange polyelectrolytes.

Angew Chem Int Ed, 2021, 60: 19272–19280
18 Marino MG, Kreuer KD. Alkaline stability of quaternary ammonium cations for alkaline fuel cell membranes and ionic liquids. ChemSusChem, 2015, 8: 513–523
19 Bai L, Ma L, Li L, *et al.* Branched, side-chain grafted polyarylpiperidine anion exchange membranes for fuel cell application. ACS Appl Energy Mater, 2021, 4: 6957–6967
20 Chen N, Hu C, Wang HH, *et al.* Poly(alkyl-terphenyl piperidinium) ionomers and membranes with an outstanding alkaline-membrane fuel-cell performance of 2.58 W cm^{-2}. Angew Chem Int Ed, 2021, 60: 7710–7718
21 Han L, Gong S, Zhang X, *et al.* Four-arm star-shaped high-performance poly(aryl piperidine) anion exchange membranes for fuel cells. J Mater Chem A, 2024, 12: 6341–6350
22 Dong H, Gu F, Li M, *et al.* Improving the alkaline stability of imidazolium cations by substitution. ChemPhysChem, 2014, 15: 3006–3014
23 Qaisrani NA, Ma L, Liu J, *et al.* Anion exchange membrane with a novel quaternized ammonium containing long ether substituent. J Membrane Sci, 2019, 581: 293–302
24 Zhang F, Li T, Chen W, *et al.* High-performance anion exchange membranes with para-type cations on electron-withdrawing C=O links free backbone. Macromolecules, 2020, 53: 10988–10997
25 Zhang F, Li T, Chen W, *et al.* Electron-donating C-NH_2 link backbone for highly alkaline and mechanical stable anion exchange membranes. ACS Appl Mater Interfaces, 2021, 13: 10490–10499
26 Jiang Z, Yi G, Yao X, *et al.* Durable and highly-efficient anion exchange membrane water electrolysis using poly(biphenyl alkylene) membrane. Chem Eng J, 2023, 467: 143442
27 Pang Y, Li Q, Liu B, *et al.* Bis-cationic crosslinked anion exchange membranes based on carbazole-containing polyaromatics with excellent ionic conductivity for alkaline water electrolysis. Chem Eng J, 2024, 499: 156473
28 Zhang J, He Y, Zhang K, *et al.* Cation–dipole interaction that creates ordered ion channels in an anion exchange membrane for fast OH^- conduction. AIChE J, 2021, 67: e17133
29 Trigg EB, Gaines TW, Maréchal M, *et al.* Self-assembled highly ordered acid layers in precisely sulfonated polyethylene produce efficient proton transport. Nat Mater, 2018, 17: 725–731
30 Hu S, Hu L, Zhu X, *et al.* Chiral V-shaped pyrenes: hexagonal packing, superhelix, and amplified chiroptical performance. Angew Chem Int Ed, 2021, 60: 19451–19457
31 Ritter JR, Caldas MJ, da Silva TJ, *et al.* Surface effects on pyrene luminescence excitation. ACS Appl Electron Mater, 2020, 2: 2806–2812
32 Takaya T, Oda T, Shibazaki Y, *et al.* Excited-state dynamics of pyrene incorporated into poly(substituted methylene)s: effects of dense packing of pyrenes on excimer formation. Macromolecules, 2018, 51: 5430–5439
33 Lu T, Chen F. Multiwfn: a multifunctional wavefunction analyzer. J Comput Chem, 2012, 33: 580–592
34 Lu T, Chen Q. Independent gradient model based on Hirshfeld partition: a new method for visual study of interactions in chemical systems. J Comput Chem, 2022, 43: 539–555
35 Cha MS, Park JE, Kim S, *et al.* Poly(carbazole)-based anion-conducting materials with high performance and durability for energy conversion devices. Energy Environ Sci, 2020, 13: 3633–3645
36 Chen J, Guan M, Li K, *et al.* Highly hydroxide-conductive anion exchange membrane with PIL@MOF-assisted ion nanochannels. J Industrial Eng Chem, 2021, 94: 465–471
37 Chen N, Wang HH, Kim SP, *et al.* Poly(fluorenyl aryl piperidinium) membranes and ionomers for anion exchange membrane fuel cells. Nat Commun, 2021, 12: 2367
38 Fan Y, Zhou J, Chen J, *et al.* Polyaryl piperidine anion exchange membranes with hydrophilic side chain. Int J Hydrogen Energy, 2023, 48: 17630–17640
39 Ge Q, Liu Y, Yang Z, *et al.* Hyper-branched anion exchange membranes with high conductivity and chemical stability. Chem Commun, 2016, 52: 10141–10143
40 Gong S, Han L, Zhang X, *et al.* Adjusting the perfluorinated side chain length in dual-grafted anion exchange membranes for high performance fuel cells. J Mater Chem A, 2024, 12: 4184–4194
41 Liu L, Bai L, Liu Z, *et al.* Side-chain structural engineering on poly(terphenyl piperidinium) anion exchange membrane for water electrolysers. J Membrane Sci, 2023, 665: 121135
42 Ma Y, Hu C, Yi G, *et al.* Durable multiblock poly(biphenyl alkylene) anion exchange membranes with microphase separation for hydrogen energy conversion. Angew Chem, 2023, 135: e202311509
43 Song W, Peng K, Xu W, *et al.* Upscaled production of an ultramicroporous anion-exchange membrane enables long-term operation in electrochemical energy devices. Nat Commun, 2023, 14: 2732
44 Wu X, Chen N, Hu C, *et al.* Fluorinated poly(aryl piperidinium) membranes for anion exchange membrane fuel cells. Adv Mater, 2023, 35: 2210432
45 Wu X, Chen N, Klok H, *et al.* Branched poly(aryl piperidinium) membranes for anion-exchange membrane fuel cells. Angew Chem, 2022, 134: e202114892
46 Yin L, Ren R, He L, *et al.* Stable anion exchange membrane bearing quinuclidinium for high-performance water electrolysis. Angew Chem Int Ed, 2024, 63: e202400764
47 Yuan W, Zeng L, Jiang S, *et al.* High performance poly(carbazolyl aryl piperidinium) anion exchange membranes for alkaline fuel cells. J Membrane Sci, 2022, 657: 120676
48 Zeng M, He X, Wen J, *et al.* *N*-methylquinuclidinium-based anion exchange membrane with ultrahigh alkaline stability. Adv Mater, 2023, 35: 2306675
49 Zhang S, Li X, Yang Y, *et al.* Microporous and low swelling branched poly(aryl piperidinium) anion exchange membranes for high-performed water electrolyzers. J Membrane Sci, 2024, 698: 122587
50 Yan X, Yang X, Su X, *et al.* Twisted ether-free polymer based alkaline membrane for high-performance water electrolysis. J Power Sources, 2020, 480: 228805
51 Zhang D, Hao W, Li J, *et al.* Anion exchange membranes from microporous poly(arylene piperidinium)-based polymers containing spirobifluorene structure. Polymer, 2025, 320: 128117
52 Cheng X, Li C, Zou X, *et al.* Highly conductive alkoxy chain cross-linked poly (aryl piperidinium) anion exchange membrane for water electrolysis. Chem Eng J, 2024, 483: 149328
53 Fang Y, Chen F, Chen X, *et al.* Enhancing OH^- conduction in poly(arylene piperidinium) anion exchange membranes with hydrophobic perfluorinated side chains. J Membrane Sci, 2025, 717: 123616
54 Liu M, Hu X, Hu B, *et al.* Soluble poly(aryl piperidinium) with extended aromatic segments as anion exchange membranes for alkaline fuel cells and water electrolysis. J Membrane Sci, 2022, 642: 119966
55 Wang J, Zhao C, Liu Z, *et al.* Durable and conductive anion exchange membranes based on poly(*m*-triphenyl carbazolyl piperidinium) for water electrolysis. Int J Hydrogen Energy, 2024, 58: 514–524
56 Li J, Li W, Wang X, *et al.* A microphase separation anion exchange membrane based on poly(terphenyl piperidinium)/cationic polyelectrolyte for high-performance AEMWEs. J Membrane Sci, 2025, 730: 124206
57 Peng Z, Wei T, Wang Q, *et al.* Fabrication and investigation of anion exchange membranes based on poly(terphenyl piperidonium) copolymers with dibenzothiophene or dibenzofuran units for water electrolysis. J Power Sources, 2025, 642: 236918
58 Hu C, Lee JY, Lee YJ, *et al.* Reinforced poly(dibenzyl-*co*-terphenyl piperidinium) membranes for highly durable anion-exchange membrane water electrolysis at 2 A cm^{-2} for 1000 h. Next Energy, 2023, 1: 100044
59 Chen N, Paek SY, Lee JY, *et al.* High-performance anion exchange membrane water electrolyzers with a current density of 7.68 A cm^{-2} and a durability of 1000 hours. Energy Environ Sci, 2021, 14: 6338–6348
60 Hu C, Kang HW, Jung SW, *et al.* High free volume polyelectrolytes for anion exchange membrane water electrolyzers with a current density of 13.39 A cm^{-2} and a durability of 1000 h. Adv Sci, 2024, 11: 2306988

Acknowledgement This work was supported by the National Key R&D Program of China (2022YFA1504003), the National Natural Science Foundation of China (22322811, 22278388, 223B2804, and 22438012), and the University Synergy Innovation Program of Anhui Province (GXXT-2022-027). The calculation was performed on the supercomputing system in the

Supercomputing Center at the University of Science and Technology of China.

Author contributions Xu T, Ge X, Wu L and Wang Y conceived the idea and directed the project. Yang C designed experiments, performed the measurements and the analysis, and wrote the manuscript with the support from Xu T, Ge X and Song W. Huang Y completed the theoretical calculations and relevant data analysis. Nie J and Wu M performed relevant measurements and analyzed data. All authors contributed to the general discussion.

Conflict of interest The authors declare that they have no conflict of interest.

Supplementary information Supplementary materials are available in the online version of the paper.

Cui Yang received her BE degree from Hefei University of Technology in 2020. She is currently a doctoral candidate at the University of Science and Technology of China. Her research interests focus on anion exchange membranes, polymer chemistry, and water electrolysis.

Yu Huang received his BE degree from the University of Science and Technology in 2022. He is currently a doctoral candidate at the University of Science and Technology of China. His research interests focus on multiscale theoretical simulation of soft matters.

Xiaolin Ge received his BE, ME, and PhD degrees from Henan University of Science and Technology, China, in 2010, Hefei University of Technology, China, in 2013, and the University of Science and Technology of China in 2016. He is working at the Department of Applied Chemistry, School of Chemistry and Materials Science, University of Science and Technology of China, Hefei, China. His research interests focus on ionic membranes, polymer chemistry, and supramolecular chemistry.

Tongwen Xu received his PhD degree in chemical engineering from Tianjin University. He has been a professor at the University of Science and Technology of China since 2002. He has been a fellow of the Chinese Chemical Society since 2024, a fellow of the Chemical Industry and Engineering Society of China since 2020 and a fellow of the Royal Society of Chemistry since 2013. His interests are ion exchange membranes and related processes, membrane structure designs and fabrications, and aqueous flow batteries.

利用芘单元堆叠骨架提高水电解AEM的OH^-电导率和耐碱稳定性

杨翠[1†], 黄渝[2†], 宋晚杰[1], 吴明玥[1], 聂瑾玉[1], 汪耀明[1], 吴亮[1], 葛晓琳[1*], 徐铜文[1*]

摘要 由于具有良好的商业前景，基于阴离子交换膜(AEMs)的新兴制氢技术引起了越来越多的关注. 然而, 其在离子电导率和耐久性方面仍存在挑战. 本文介绍了一种新型的方法, 通过π-π相互作用来增强AEMs的耐碱稳定性、提高氢氧根离子电导率. AEMs中的π-堆积诱导阳离子聚集, 促进微相分离形态的形成, 从而提高局部离子浓度, 强化离子表面跳跃位点. 除此之外, 芘的给电子效应可以有效降低邻近季铵离子上的β-H的静电势，达到提高OH^-亲核攻击反应能垒的效果. 所制备的AEMs具有优异的性能，在兼具高电导率(160 mS/cm)的同时展现了优异的耐碱稳定性(在80 °C的2 M KOH中老化1950 h后，电导率仅下降0.35%). 在此基础上，在电解水膜电极组件测试中在1.8 V获得了2.58 A/cm^{2}的电流密度，同时在耐久性测试中保持了700小时以上的稳定运行.

